Influence of Central Sidechain on Self-Assembly of Glycine-X-Glycine Peptides

Influence of Central Sidechain on Self-Assembly of

Glycine-X-Glycine Peptides

Lavenia J. Thursch[1], Thamires A. Lima[1], Nichole O'Neill[1,3], Fabio Furlan

Ferreira[2], Reinhard Schweitzer-Stenner[3]*, and Nicolas J. Alvarez[1]*

[1]Department of Chemical and Biological Engineering, Drexel University,

Philadelphia, PA 19104, USA, [2]Centro de Ciências Naturais e Humanas,

Universidade Federal do ABC, Santo André, São Paulo, Brazil and

[3]Department of Chemistry, Drexel University, Philadelphia, PA 19104, USA

To be submitted to: *Soft Matter*

1

*Corresponding authors: N.J.A.: Phone: 215-571-4120; Email: nja49@drexel.edu and

R.S.S: Phone: 215-895-2268; Email: rschweitzer-stenner@drexel.edu

Abstract

Low molecular weight gelators (LMWG) are the subject of intense research for a range of

biomedical, and engineering applications. Peptides are a special class of LMWG, which

offer infinite sequence possibilities and, therefore, engineered properties. This work

examines the propensity of the GxG peptide family, where x denotes a guest residue, to

self-assemble into fibril networks via changes in pH and ethanol concentration. These

triggers for gelation are motivated by recent work on GHG and GAG, which unexpectedly

self-assemble into centimeter long fibril networks with unique rheological properties. The

propensity of GxG peptides to self-assemble, and the physical and chemical properties

of the self-assembled structures are characterized by microscopy, spectroscopy,

2

rheology, and X-ray diffraction. Interestingly, we show that the number, length, size, and

morphology of the crystalline self-assembled aggregates depend significantly on the x-

residue chemistry and the solution conditions, i.e. pH, temperature, peptide

concentration, etc. The different x-residues allow us to probe the importance of different

peptide interactions, e.g. $\pi - \pi$ stacking, hydrogen bonding, and hydrophobicity, on the

formation of fibrils. We conclude that fibril formation requires $\pi - \pi$ stacking interactions

in pure water, while hydrogen bonding can form fibrils in the presence of ethanol-water

solutions. These results validate and support theoretical arguments on the propensity for

self-assembly and leads to a better understanding of the relationship between peptide

chemistry and fibril self-assembly. Overall, GxG peptides constitute a unique family of

peptides, whose characterization will aid in advancing our understanding of self-assembly

driving forces for fibril formation in peptide systems.

Introduction

Over the last twenty years short and ultrashort peptides have emerged as building blocks

of self-assembled structures such as nanotubes, nanowires and fibrils capable of forming

3

sample spanning networks that lead to gelation of the sample.[1–8] These supramolecular

structures are strong candidates for drug delivery and biotechnology applications such as

tissue scaffolding.[9,10] Short peptides offer several advantages over other low molecular

weight gelators, such as, cytocompatibility, low toxicity, and relatively low production

costs.[11,12]

The ability of short peptides to self-assemble depends strongly on their amino acid

residue sequences. For example, It has been argued that self-assembly of oligopeptides

requires a certain number of residues (e.g. 10 for alanine based oligopeptides) as well as

a certain degree of amphiphilicity, i.e. sequences with alternating hydrophobic and

hydrophilic residues.[2,13–15] Classical examples are the thoroughly investigated and

characterized RADA16 and EAK 16.[15–19] Oligopeptides with a net charge generally

require a pH-change as trigger of the self-assembly process,[20,21] but exceptions from the

rule have been reported.[22–24]

The above outlined rules have been challenged by the discovery that aromatic

amino acid residues containing ultrashort oligopeptides can produce a variety of

supramolecular structures. For instance, Gazit and associates investigated a hexapeptide segment NFGAIL of the islet amyloid polypeptide and found that phenylalanine (F) and tryptophan (W), both aromatic residues, were necessary to induce the self-assembly of the peptide sequence; peptide derivatives with aliphatic residues, e.g. alanine, did not self-assemble into detectable aggregates.[25] F and W are both aromatic, and there is evidence that π-π stacking interactions are involved in their propensity for aggregation.

[26,27]

Subsequent studies have underscored phenylalanine's propensity for self-assembly of even short peptide fragments. For example, the two phenylalanine residues in the $A\beta_{16-20}$ fragment are responsible for its amyloid forming capability.[28] Reches and Gazit showed that phenylalanine dipeptides (FF) can self-assemble into various supramolecular structures, including nanowires and gel forming sample spanning networks.[29] This discovery initiated a large number of investigations that used FmocFF (Fmoc: fluorenylmethyloxycarbonyl) and boc-FF (boc: N-(tert-butoxycarbonyl) peptides as well as their derivatives as low molecular weight gelators.[30,31] Depending on the

5

respective amino acid residue composition and solvent parameters the obtained gels were generally of moderate strengths with storage moduli in the range of 10^3-10^4 Pa. All the gel phases have in common that the sheets of the underlying fibrils exhibit β-sheet structures.

A notable study by Frederix et al. screened the entire landscape of tripeptides via molecular dynamics simulation for the most likely combination of amino acid residues to self-assemble in water.[32] They found that tripeptides containing tryptophan, phenylalanine and tyrosine (Y) residues has the highest propensity for aggregation. The respective propensity for histidine (H), which contains an aromatic side chain as well, depends on the remaining two amino acid residues of the tripeptide. If histidine is the central residue aromatic and most aliphatic residues at the N-terminal produced high propensity scores for most of the C-terminal residues, while alanine (A), glycine (G), glutamate (Q) and asparagine (N) were linked to much lower scores. When glycine is placed at the N-terminal of the tripeptide, the presence of serine (S), threonine (T), tyrosine or phenylalanine as C-terminal neighbor was tantamount to gain significant

6

aggregation propensity. The propensity of GHG was predicted to be very low. Many other residues need support from aromatic neighbors to exhibit significant propensity; this notion particularly applies to glycine (G) and alanine (A).

The solvent quality is a major factor in the propensity of peptides to self-assemble into gels. For example, we showed that the cationic GAG could form a gel in water/ethanol [33], and that GHG readily formed long macrofibril hydrogels in water upon the deprotonation of its imidazole side chain.[34] Both gels result from the physical entanglement of centimeter long crystalline fibrils. The density of fibrils, homogeneity of entanglements, and the stability of the fibrils are linked to the formation conditions, and the solution properties (namely, pH and temperature) after formation.[8] In many ways, these GxG fibril hydrogels differ from other ultra-low molecular weight gelators (ULMWGs) such as FmocFF. For example, the critical gel concentrations lie in the centimolar and sub-molar range. They are thus substantially higher than the critical concentrations of FmocFF and its derivatives. GAG and GHG gel phases are underlied by a network of ultra-large crystalline fibrils, with a diameter of about a micrometer and

up to a centimeter in length. [35,36] These networks have exciting mechanical properties

with storage moduli in the 10^5 Pa regime. Spectroscopic evidence strongly suggests that

the secondary structure of the fibril forming peptide sheets and tapes differ significantly

from canonical β-sheet structures. The vibrational dichroism profiles of these peptides'

amide I modes reflect a high degree of fibril chirality.[37,38] For GAG we found a phase

transition between two gel phases of different fibril chirality,[33] in line with earlier reported

gel <-> gel transitions.[39,40] The melting of its gel phases is a non-reversible process.

The unexpected self-assembly and unique properties of GAG and GHG peptide

hydrogels raises questions regarding the molecular interactions that promote the self-

assembly into crystalline fibrils over the formation of dense disordered aggregates.

Therefore, this work investigates whether other GxG peptides with aromatic, aliphatic and

ionizable side chains (see Figure 1), i.e. GYG, GWG, GFG, GVG, GPG, GKG and GDG

can self-assemble into similarly long crystalline fibrils for peptide concentrations in the

sub-molar range. We are particularly interested in comparing the self-assembly of

aromatic amino acid guest residues with the one of the forementioned GAG and GHG. In

addition, our aim is to investigate under which conditions self-assembly is favored for a

given x-residue, and the physical and chemical properties of the formed structures. All

tripeptides were screened for self-assembly in aqueous and water/ethanol phases.

Spectroscopy and microscopy were both employed to characterize the kinetics of the

peptides' self-assembly and gelation and the microstructure of formed gels. Finally, we

present the solved crystalline structures of GDG, GHG, GYG, and GAG precipitated

peptide powder and compare them to the diffraction powders of their respective

hydrogels. Note that to the best of our knowledge, there are no previous studies

presenting the structure of these tripeptide powders.

Materials and Methods

Peptides

Unblocked peptides glycyl-alanyl-glycine (GAG), Glycyl-histidyl-glycine (GHG), Glycyl-aspartyl-glycine (GDG), Glycyl-lysyl-glycine (GKG), Glycyl-phenylalanyl-glycine (GFG), Glycyl-prolyl-glycine (GPG), Glycyl-tryptophyl-glycine (GWG), Glycyl-tyrosyl-glycine (GYG), and Glycyl-valyl-glycine (GVG), were purchased in the form (H-Gly-Xxx-Gly-OH), from Bachem with >99% purity and used as received.

Gel preparation

pH Induced Gelation: The hydrogels were prepared by first adding deionized water to the as-received peptide powder, then hydrochloric acid (HCl) 50% vol (ACS grade, Ricca Chemical Company) to protonate the peptide and ensure its quick dissolution in the aqueous phase. Finally, a 2.24 M sodium hydroxide solution (commercial solution Ricca Chemical Company, diluted 10 times) was added to deprotonate the carboxylate group

of the peptide and trigger self-assembly. In the case of GHG gelation additionally required

the deprotonation of the imidazole side chain.

Solvent Induced Gelation: We also prepared water and ethanol-based samples by either

(1) dissolving the as-received peptide powder in deionized water and HCl and adding

ethanol (200 proof, Pharmco-Aaper) to trigger gelation or (2) mixing the peptide in a

water/ethanol solvent phase and then adding HCl.

Deuterated reagents D_2O (99.9% purity, Sigma Aldrich), ethan(ol)-d (EtOD, 99.9% purity,

Sigma Aldrich), as well as deuterium chloride (Sigma Aldrich) and sodium deuteroxide

(NaOD) (Sigma Aldrich) were used as reagents for Fourier transform Infrared

spectroscopy (FT-IR) experiments to avoid the overlap of the strong water band at 1640

cm^{-1} with the amide I region (1600-1700 cm^{-1}).

Microscopy

Pictures of the gels were captured on an Amscope 7X-45X Trinocular Stereo Zoom

microscope equipped with an Amscope MU130 camera or alternatively with a Jiusion 40X

11

to 1000X digital microscope. We also installed a modular microscope accessory on the rheometer to acquire brightfield images during the gel formation and melting steps. The accessory was provided by TA Instruments and consists of a 3D translation microscope stage with an optical glass plate mounted on a stand that replaces the standard shear rheology aluminum bottom plate. The camera used was the digital microscope mentioned above.

FTIR spectroscopy

FTIR experiments were carried out using the ATR set up of a Thermo Nicolet Nexus 870 FT-IR spectrometer in absorbance mode. Spectra were recorded with 32 scans at a 4 cm^{-1} resolution at room temperature with a deuterated triglycine sulfate (DTGS) detector in 650−4000 cm^{-1} range for mid-infrared (M-IR) spectra. The gels were prepared as previously described, and the data were collected over time to probe the gel formation kinetics. Part of the observed IR spectra in the region from 1400-1800 cm^{-1} were decomposed into individual Gaussian bands in (amide I' region) and Voigtian bands (COO^- antisymmetric stretching) using the MULTIFIT software[41] and an in-house spectral

12

decomposition program written in Matlab® (Mathworks Inc.). The decomposition also

accounted for a Voigtian character in the lowest-wavenumber amide I' band. A

justification for the choice of band profiles is given in the Result section. The MULTIFIT

fitting routine has an internal check to determine when the fit is satisfactory. Both fitting

routines utilized least squares procedures. The fractional intensity (I_{rel}) of an AI' band

was plotted as a function of time using the ratio between the band intensity (I) and the

total intensities of the bands fitted in the AI' region ($\sum I_n$).

$$I_{rel} = \frac{I}{\sum I_n} \tag{1}$$

Rheology

Rheology measurements were obtained on a DHR-3 rheometer (TA instruments) using a

Peltier plate for temperature control with a 25 mm diameter top plate. Each measurement

consisted of 400 μL of peptide solution. A gap of 700 μm was applied for all experiments.

A solvent trap was devised using safflow safflower oil around the free surface edge of the

sample to minimize evaporation. The ethanol/water solutions were confirmed to have little to no solubility in safflower oil. All samples were prepared one to three minutes prior to loading. The exact time between adding of the last reagent and the beginning of the rheology experiment was recorded as time zero and accounted for during data treatment.

The mechanical properties of the hydrogel were probed by small amplitude oscillatory shear (SAOS) measurements. The storage and viscous modulus were measured using SAOS as a function using 25 mm parallel plates with a strain of 0.03 %, and an angular frequency of 1 rad/s.

X-ray Diffraction

X-ray powder diffraction data of GXG powder and gel were collected at room temperature on a STADI-P powder diffractometer (Stoe®, Darmstadt, Germany), in transmission geometry (the samples were loaded between two cellulose acetate foils and held spinning during data collection), with monochromatic $CuK\alpha_1$ (λ = 1.54056 Å) wavelength selected by a curved Ge (111) crystal, operating at 40 kV and 40 mA. The diffracted intensities

were collected by a silicon microstrip detector, Mythen 1K (Dectris®, Baden, Switzerland),

in the range from 6.000° to 87.885°, with 50 s of integration time at each 1.05º for GAG,

GDG; from 4.000° to 92.185°, with 300 s of integration time at each 1.05º for GAG gel;

from 3.000° to 88.035°, with 200 s of integration time at each 1.05º for GDG gel, GFG

gel, GWG gel, and GYG gel; from 2.000° to 90.185°, with 50 s of integration time at each

1.05º for GFG; from 6.000° to 91.035°, with 50 s of integration time at each 1.05º for GHG;

from 6.000° to 87.885°, with 200 s of integration time at each 1.05º for GHG gel; from

3.000° to 97.845°, with 50 s of integration time at each 1.05º for GWG and from 4.000° to

95.335°, with 50 s of integration time at each 1.05º for GYG.

15

Results

Screening for visible aggregates.

The capability of an oligopeptide to self-assemble into a gel-forming network is linked to its solubility.[4,42,43] If the concentration of a peptide exceeds its solubility the solution becomes supersaturated and the peptides either disordered precipitate or form structured aggregates that can further assemble into a gel at suitable conditions.[4,44] Previously, we showed that the tripeptide GHG could form a gel in water upon the deprotonation of its imidazole side chain at pH value above 6.[36,45] Before self-assembly, the peptide was dissolved by lowering the pH below three, to ensure solubility via the protonation of the C-terminal carboxylate group and of the imidazole side chain. Subsequently, the sample was titrated with NaOH to different pH values above the critical gelation value. The critical gelation concentration of deprotonated GHG was found to lie between 40 and 50 mM.[36,46] A different protocol was employed to trigger the self-assembly and gelation of GAG by the titration of ethanol into a solubilized peptide solution. The tripeptide GAG forms long entangled fibrils in a water/ethanol solution at acidic pH. The critical concentration varies

16

with the ethanol content between 75 mM in 74 mol% ethanol/26 mol% water and 350 mM

in 34 mol% ethanol/66 mol% water at room temperature.[35] The self-assembly was

triggered by adding ethanol to the dissolved peptide in water or alternatively by adding a

water/ethanol solution to the peptide and dissolving with HCl.

These two protocols, i.e. cyclic pH change and ethanol addition, were adopted in

this study to screen other GxG tripeptides for self-assembly. This strategy was motivated

by the observation that C-terminal protonation generally increases the solubility of GxG

peptides in water. In line with expectations, we could dissolve ca. 100 mM of all peptides

investigated (Table 1) at acidic pH values below the pK of the respective C-terminal

carboxylate group. Self-assembly were induced by either adding 55 mol% ethanol or

NaOH to the sample. We expected that the change in pH or an increased ethanol fraction

(an anti-solvent) would reduce the solubility of the peptide and thus trigger self-assembly

into crystalline aggregates. This protocol worked as expected for GDG, GFG and GYG

for which we had to increase the pH to values around 4 in order to achieve the formation

of visible aggregates. For 75 mM GWG, however, we already observed visible aggregates

17

at a pH of 0.9. Table 1 lists the peptide concentrations and pH values at which self-assembly and gelation was obtained. Our results suggest that unlike in the case of GHG, the protonation of the C-terminal residue of GDG, GFG and GYG peptides triggers self-assembly into visible crystalline fibrils/aggregates. GVG, GKG and GPG could be dissolved in deionized water without lowering the pH (80 mM, 115 mM, and 110 mM respectively). When gradually raising the pH to about 11 to 12, the solution remained clear and no visible aggregation was observed. This result suggests that the deprotonations of their basic groups (lysine side chain and the N-terminal ammonium groups) do not lower their solubility to a sufficient extent. For the case of ethanol/water solutions, we observed the self-assembly of 75 mM GDG and 100 mM GFG. The other peptides investigated either did not dissolve in water or water/ethanol at appreciable concentrations (e.g. GWG, GYG) or dissolved but showed no evidence of self-assembly over several days (e.g. GKG, GPG, GVG).

In summary, GxG peptides with x=D, H, F, and Y self-assemble via an increase in pH after dissolution at low pH, while GWG forms visible crystalline fibrils already at acidic

18

pH where the C-terminus is protonated. GxG peptides with x=A, D, and F also form fibrils upon the addition of ethanol as an anti-solvent. Peptides with x=K, P, and V did not form any observable self-assembled aggregate structures under the conditions studied. It is somewhat surprising that GVG did not self-assemble in water or water/ethanol solutions given its hydrophobicity being higher than GAG.[47]   The remainder of the paper is organized by characterization technique, detailing the dynamics/kinetics of formation and macro and crystalline structures of the GxG self-assembled aggregates.

Microscopy

Figure 2 shows an overview of the various macro structures formed by the self-assembled GxG aggregates. Figure 2a and 2j show that GDG forms comparatively short crystalline fibrils in water and in water/ethanol. This observation is further denoted by rheology experiments, which revealed no aggregate connectivity for this peptide *(vide infra)*. To the contrary, GFG forms significantly long sample spanning crystalline fibrils in the pH induced self-assembly (Figures 2b and 2f), but comparatively shorter, fatter, and less

19

entangled crystalline fibrils in 55 mol% ethanol (Figure 2k). GWG at low concentrations

(Figure 2c) forms a fibril network like that of GFG, but upon increasing the peptide

concentration from 75 mM to 200 mM (Figure 2g) the fibrils become shorter and form

discontinuous dense aggregates. The latter is an indicator of liquid-liquid demixing[48] and

have been linked in our previous work to fast self-assembly kinetics.[35,49] The fibril and

fibril microstructure of GFG and GWG water aggregates resembles that of the loose,

highly entangled fibril hydrogels formed by GAG (Figure 2i) while they differ from the

highly ordered, haystack structures formed by GHG in water (Figures 2e and 2i). Lastly,

GYG aggregates are peculiar in that they resemble spherical colloidal aggregates (Figure

2d), which interact or percolate at higher concentrations (Figure 2h). The range and

breadth of the micro and macro self-assembled structures in the GxG peptide family

provide a rich parameter space to develop biomedical applications and study the

interactions between living cells and peptide crystalline fibrils.

FTIR spectroscopy and kinetics of sheet formation.

20

The initial phase of self-assembly of GFG (pH= 3.4 and 3.8), GWG (pH = 0.7), and GYG

(pH= 4.1) were probed using FTIR spectroscopy. The formation of sheet-like structures

predominantly affects the amide I band position in the respective IR spectra due to

interstrand vibrational coupling.[50–52] The subsequent self-assembly into tapes and fibrils

has a more limited influence.[33] In the case of the canonical β-sheet formation, interstrand

vibrational interactions disperses amide I intensities over a large spectral region between

1610 and 1690 cm^{-1}.[51–53] Most of the oscillator strength is concentrated in very few

overlapping bands positioned at the low wavenumber end of this region. Recently we

demonstrated the peculiar amide I pattern formed by GAG crystalline fibrils in water-

ethanol, namely the split of a broad, unstructured amide I band for the monomer into two

sharp bands that to some extent resemble the pattern for single crystals of diglycine.[33,54]

Density functional theory calculations revealed that this pattern can indeed be explained

with the aggregation into sheets which differ significantly from classical β-sheets.[55]

Furthermore, the sheet formation of GHG in water gives rise to an amide I dispersion

21

where the intensity is distributed over at least four different bands,[45] which also indicates

a departure from classical β-sheet dispersions.

Figure 3 shows the IR spectra for GFG, GWG, and GYG in the region from 1550

to 1750 cm^{-1} as a function of time. The spectral region below 1600 cm^{-1} was fit with

Gaussian profiles using MultiFit, while Voigtian profiles had to be employed for the amide

I' region (the prime sign indicates deuterated amide group in D_2O). Gaussian profiles are

an arbitrary choice for the decomposition of vibrational bands in the liquid phase.

However, in an ordered and more homogeneous phase like crystals, Lorentzian profiles

are considered a better choice. The need for Voigtian profiles indicates that the carbonyl

groups sample inhomogeneity in the self-assembled structure, and/or that individual

bands represent clusters of excitonic transitions.[56] The necessity to use a Gaussian

profile for the COO^--band indicates the rotational flexibility of the C-terminal carboxylate

group.[57] Note that exact determination of the spectral composition is difficult with an ATR

setup given the random orientation of crystalline domains in the cell. Thus, in this work

we focus on quantifying spectral changes rather than on an exact determination of the

22

spectral composition. For spectral composition deconvolution, we showed recently that a

thin transmission cell is advantageous.[56]

The kinetic plots in Figure 4 depict the integrated fractional intensities of the AI'

bands (i.e. normalized on the total amide I' intensity) as a function of time. These

intensities were obtained using a self-consistent approach, where the first spectrum (time

equals zero) was used to fit band positions, halfwidths and integrated intensities. Next,

fixed wavenumbers and halfwidths were used for all subsequent spectra, except for a few

cases where the wavenumber positions were allowed to vary slightly to optimize the

fitting.   Representative decompositions of the last spectra measured at the end of the

kinetic experiments are shown in Figure S1.

In the spectra of GFG and GYG, the very intense band close to 1600 cm^{-1} must be

assigned to the COO^- antisymmetric stretching mode of the deprotonated C-terminal.[58] In

the spectrum of GWG, it is replaced by a band at 1715-1730 cm^{-1}, which is assignable to

the carbonyl stretching mode of the protonated C-terminal. The former is initially rather

broad, and blueshifts and narrows over time. Our analysis indicates that it is composed

23

of two bands. Over time the band at higher wavenumbers gains intensity over the one at

lower wavenumbers. This strongly suggests that either the COO^- group is transferred to

a different (less hydrated) environment over time and/or an overlap with the red shifting

amide I' profile of the fibril spectra. All the other bands in the spectrum can be assigned

to amide I'.

It is important to note that the amide I profile overlaps with the spectral

contributions from monomers and shorter oligomers. Thus, the spectral decomposition

into four (for GFG and GWG) and five sub-bands (for GYG) (cf. Table 2) should be

considered as heuristic, since at least the amide I' profile measured at the end of the time

window is likely to predominantly represent a single (crystalline) conformation which gives

rise to a specific amide I dispersion. Interestingly, the spectral evolutions of GFG and

GYG very much resemble the one earlier obtained for GHG. There is no doubt that the

respective AI_1'-sub-band below 1635 cm^{-1} is an indicator of sheet formation, even though

the latter is not of the β-sheet type. The amide I' dispersion of GWG is very similar to the

GAG in water/ethanol spectrum, though with a larger splitting between the two dominant

24

sub-bands. The low wavenumber band of the GWG is at 1640 cm^{-1}, while it is at 1647

cm^{-1} for GAG.

Among the amide I' sub-bands, only the low wavenumber band can be used as an

indicator of sheet formation kinetics, which are shown in Figures 4a and 4b. The

experimental data observed for GFG and GWG were fitted to the following exponential

equation by employing the non-linear least square software using Sigma Plot ® :

$$I(\tilde{\nu}) = I_{max}(1 - e^{-\frac{t}{\tau}})\ \ \ \ \ \ \ \ (2)$$

where I_{max} is the value at which the kinetics level off and τ is the apparent time constant

of sheet formation. The fit to the kinetics observed for GWG at pH 0.7 required a fit with

two exponential functions (Table 2). We would like to emphasize that our approach is

heuristic in nature and does not reflect a specific kinetic model. We just aim at obtaining

apparent time constants that can be used for comparison with the kinetics of gelation

described below. We showed earlier that a mono-exponential function is well suited to

describe the kinetics of the self-assembly of GAG in water-ethanol.[33]

25

The parameter set obtained from the fits in Figure 4 is all listed in Table 2.

Figure 4 summarizes the kinetic self-assembly for GFG, GWG, and GYG. The kinetic results in Figures 4a and b elucidate the pH sensitivity of the GFG self-assembly process. At pH 3.4 the kinetics level off after ca. 60 mins, the corresponding time constant is 21.69 s. However, at pH 3.8 our experiment missed on a very fast self-assembly phase that exists outside the experimental window (Figure 3b). The spectra in Figure 3 as well as the I_{max} – values in Table 1 suggest that more peptides become incorporated in sheets at pH 3.8, compared to pH 3.4. Table 2 summarizes the best fit parameters of Eq. 1. The IR spectra lack a CO band above 1700 cm $^{-1}$ suggesting GFG in both gels are deprotonated. Figure 4c shows that the kinetics of GWG self-assembly is much faster than GFG at pH 3.4, but slower than GFG at pH 3.8. The best fit relaxation time for GWG is 4.24s. GYG sheets form slightly faster than GWG ($\tau = 2.5$s). While the amide I' dispersion is qualitatively similar to the one observed for GFG at pH 3.8, the AI_1 peak is less pronounced. This could be indicative of a less ordered crystal structure or of a more inhomogeneous self-assembly process that produces a mixture of fibrils coexisting with

26

an ensemble of amorphous aggregates. Such an interpretation is consistent with the

spherical morphology of GYG aggregates.

Rheology

Figure 5a shows the gel phase formation kinetics monitored by rheology for GFG, GWG

and GYG samples. We can confirm that these samples formed a gel network with the

storage modulus G' higher than the loss modulus G'' for all GxG samples over a large

frequency range. Apparently, the rate of gel formation and the final storage modulus

increased concomitantly with the growing homogeneity and density of fibrillar aggregates

revealed by the microscopic images on in Figure 2 (Figures 5b and c). For the 200 mM

GFG sample, we observed a storage modulus in the MPa range which is one order of

magnitude higher than previously reported for GAG and GHG (shown in Figure 5d for

comparison). The high self-assembly capability of this tripeptide is linked to the

aromaticity of the phenylalanine residue, which was previously shown to favor self-

assembly in di- and tripeptides.[32,59]   The modulus of the 100 mM GWG is in the 10^5 Pa

range and thus comparable with typical values for GAG and GHG gels, while GYG's is comparatively low, i.e. at 10^4 Pa. It is worth mentioning that GDG aggregates did not show network quality i.e., the rheology moduli were close to machine limit and $G' \approx G''$.

In addition to exploring the gelation of aromatic GxG peptides in water we measured the corresponding kinetics of 100 mM GFG in a 55 mol% ethanol/45 mol% water mixture. In the case of GAG ethanol as co-solvent decreased the peptides solubility thus facilitating supersaturation and the nucleation of peptide crystalline fibrils. The co-solvent effect on 100 mM GFG gelation is quite different in that the respective storage modulus depicted in Figure 5 plateaus at ca. 500 Pa, which is well below the value observed for the same peptide concentration in water (ca. $3 \cdot 10^4$ Pa). This observation most likely reflects the higher solubility of GFG in water-ethanol mixtures. While the solubility of phenylalanine is well below that of alanine in water it is significantly higher in 50% ethanol/50% water mixtures.[60]

The storage moduli GHG, GFG and GWG in water obtained at the higher of the respective two concentrations investigated exceed the values reported for other ultrashort

peptide gelators which generally lie in the 10^3-10^4 Pa range by one or even two orders of magnitude.[11,43,61–63] The G' value of 200 mM GFG in the MPa range is particularly noteworthy. They are also larger than the G' values reported for the gel phases of longer polypeptide gelators such as the different MAX peptides[20,21,64] and exceed by far the storage moduli of a series of 16 residue amphiphilic peptides.[24,65] Rodriguez et. al, presented G' of several MAX1 and single strand β-sheet peptide hydrogels. Among them FΔF-OH is the peptide with highest G', it exhibits a G' equal to 0.29 MPa[64,66] which is comparable with GHG, GAG and GWG and an order of magnitude lower than GFG.

We analyzed the rheology kinetics by fitting the following equation to the kinetics in Figure 5[35]:

$$G' = \frac{G'_{max}}{1 + \left(\frac{t}{\tau}\right)^a} \qquad (3)$$

This heuristic equation resembles an expression that was used to describe the relaxation of spin glasses.[67] Its sigmodal character is well suited to fit the observed relaxation kinetics. The time constant τ should be understood as representing an entire spectrum of

29

relaxation processes. The exponent *a* reflects the fractal geometry of the system. This analysis of the rheology data provides us with a maximum modulus G'_{max} and a timescale of network formation τ. The obtained parameters values seem indeed to confirm the above supposition that the storage modulus and the timescale of gelation are anticorrelated.

Generally, one would expect that the self-assembly (i.e. fibril/sheet formation) probed by the above time- resolved IR experiments precedes the gelation process. As seen in Figures 4 and 5, this is indeed the case for GYG and GWG. While the self-assembly kinetics have a half time ($\tau \cdot \ln 2$) of 4 and 3 min, respectively, the network formationτ-constants are 37 and 15 min. GFG at pH 3.8 falls into the same category in that self-assembly into crystalline fibrils is very fast (< 1 min), while the entanglement of the fibrils is on the order of 7.3 min. Interestingly, GFG at pH 3.4 behaves differently. Sheet formation proceeds with a half time of ca. 20 min, while the time constant of the corresponding gelation process is 10.2 min. This means that the network formation is nearly complete even though fibrils are still growing. It should be noted in this context that

30

the final IR spectrum of the pH 3.4 sample suggests that sheets (fibrils) and monomers/oligomers are still coexisting.

We also used rheology to investigate the thermal stability of the GFG, GWG and GYG gel phases with a concentration of 100 mM. We started with a slow increase of temperature to observe softening and melting of the gel network. The melting curves of GFG, GYG, GWG and GHG are shown in Figure. 6. Consecutively, we carried out a cooling step down to 20°C, where we measured the reformation kinetics of the gel (c.f. Figure 6). The characteristic "knee", which denotes the softening of the gel, is observed at ~30°C for GFG, ~35°C for GYG, and 40°C for GWG. GHG appears less prone to softening with a knee at about 60°C. This result suggests that the imidazole side chain of GHG adds to the stability of the gel phase. It most likely reflects the well-established capability of deprotonated imidazole to function as hydrogen bonding donor and acceptor.[68] The modulus signal becomes close to machine limit around 50°C for all gel phases, which means the connectivity between fibrils is lost although discrete fibrils may remain.

31

Interestingly, we observe a significant delay in the reformation of the GFG and GYG gel networks. We calculated the gelation timescale τ for the initial and reformed networks, see Table 3. The reformed gel storage moduli are slightly lower than the initial formation, but still the same order of magnitude. However, it takes significantly longer to form the network, τ increases from 7.3 to 23.2 min in the case of 100 mM GFG. This could be indicative of less peptides participating in self-assembly, which has been observed for GAG in water-ethanol.[35,49]

We installed a microscope attachment on the rheometer to compare the microstructure during initial formation and reformation after annealing. We recorded videos of these processes and present images extracted from the video files in Figure. 7. For both, GFG and GYG, we observe bigger crystalline fibrils after annealing and reformation. The GFG network reformed from an initial crystalline fibril that stemmed from a bubble. As time progresses (moving to the right of Figure 7), fibrils seemed to nucleate from each other and fan out from the initial fibril. This process is similar in the initial formation step, however there are significantly more nucleation sites in the initial network

formation. The initially higher flux of nuclei results in a denser network of shorter crystalline fibrils (about 2 mm in length), compared to the fewer, thicker, much longer crystalline fibrils of the reformed phase (>5 mm in length). This decrease in the number of active centers is also observable in the GYG phases. The initial formation process features dot-like solid phases in the early fibrillization stages that grow into the characteristic GYG cotton ball fibril aggregates. When annealed at 70°C and cooled down to 20°C, GYG reforms few active centers resulting in large gaps between fibrillar aggregates. We observe an initial cotton ball in the reformation dynamics, from which appears to grow additional aggregate, resulting in raspberry-like clusters. Coupling spectroscopic studies with microscopy and rheology is needed to better understand these complex reformation kinetics and structures.

X-ray Diffraction

Figure. 8 shows the X-ray diffractograms of crystalline GAG, GDG, GFG, GHG, GWG GYG as received powders and the self-assembled hydrogels (almost dried). Glusker and

33

coworkers previously investigated the crystal structure of pure GFG. They reported the

crystal structure of GFG single crystals as orthorhombic with space group $P2_12_12_1$ and

unit cell parameters a = 29.72 Å, b = 9.98 Å, and c = 4.90 Å.[69,70] However, to the best of

the authors' knowledge, this is the first report of crystalline structures for GAG, GDG,

GHG and GYG in the literature. Figure. 9 and S2 show the crystalline unit cells for the

structures obtained in this study, and the Rietveld plots of each, respectively. The lattice

parameters obtained are shown in Table 4. Most structures are orthorhombic, space

group $P2_12_12_1$, except for GHG, which shows a monoclinic structure, space group $P2_1$,

presenting β = 104.95°. All orthorhombic structures present four peptide molecules per

unit cell, while the monoclinic ones exhibit only two GHG molecules and two water

molecules per unit cell. None of the peptides in the unit cells shown in Figure 9 adopted

a β-strand structure.

We can compare these crystalline cells to an amyloid-forming peptide sequence,

AAAK, of the 12-residue peptide: KFFEAAAKKFFE. The crystal structure of this

sequence was investigated by Makin *et al.* and was found to belong to the $P2_12_12_1$ space

34

group with a = 9.52 Å, b = 21.3 Å, and c = 48.1 Å. They observed antiparallel β-sheet

arrangements with 4.76 Å between β-strands and 9.5 Å between β-sheets. This is very

similar to the crystalline parameters observed here. Another similarity is the arrangement

of the nearby parallel stacking of aromatic groups, i.e. π-π stacking, which is an

energetically favored protein packing. The structures of the GxG gels are still under

investigation but are presented here for comparison. Figure S3 shows a clearer

comparison between the raw diffractograms of the dried gels and powders for each

peptide (5° < 2θ < 50°). Analyzing the presence/absence of Bragg peaks and their

positions suggests that GDG and GHG gels (dried) present the same crystalline structure

as the pure powder, while the GAG, GFG, GWG, and GYG have completely different

structures in the gel (dried) and powder phase. Their best fit structure will be the subject

of future investigations. The Crystallographic Information File (.cif) and the fractional

coordinates, bond lengths and angles, and hydrogen bonds for the structures determined

herein can be found as Supplementary materials. The .cif were also submitted to The

Cambridge Crystallographic Data Centre- CCDC (GAG- 2129519, GYG-2129520, GDG-

2129521 and GHG- 2129522).

Discussion

In this study, we provide a more comprehensive picture of the self-assembly and

gelation of selected GxG tripeptides. Earlier results obtained for cationic GAG in water-

ethanol mixtures and GHG in water suggested that by titrating samples of solubilized

peptides towards supersaturation produces bundles/domains of extraordinary long

crystalline fibrils due to liquid-liquid demixing and phase separation.[35,45,49] At sufficiently

high concentrations, the fibrils would form a sample spanning network, denoted as the

gel phase (Figure 2). For both peptides solubilization required switching the pH of the

sample to values below the pK-values of the respective C-terminal carboxylate group.

Supersaturation was then achieved by adding ethanol as co-solvent (for GAG) or by the

addition of NaOH to a pH above the pK value of the carboxylate group (for GFG and

GYG) or the imidazole side chain (for GHG). The high density of fibrils in the gel phase is

36

denoted by the large storage moduli particularly for GHG and GFG (Figure 5). The

gelation of GWG at pH 0.8 is surprising. We speculate that the gelation might have been

triggered by the rather high ionic strength at such a low pH, but further experiments are

necessary to shed some more light on our observation. GDG shows a peculiar behavior

in that it self-assembles into long fibrils in its zwitterionic state where side chain of the

guest residue is still protonated while these fibrils do not assemble into a gel supporting

network.

Generally, self-assembly of proteins and peptides into gels can be achieved in two

ways: (1) phase separation into droplets followed by gelation inside the secondary droplet

phase, or (2) gelation without phase separation.[48] The latter is known to cause

intracellular phase transitions that lead to the formation of membrane-less condensates,

such as the sparse fibril networks shown in Figure 2.[71] It is evident from Figure 2 that

GxG peptides are capable of forming both (1) and (2) type gels. For example, GDG and

GYG form condensed aggregate phases, with little to no overlap, while GFG, GWG, and

GHG all form sparse interconnected fibril networks. Therefore, the question arises

37

whether specific interactions are necessary to induce fibril aggregates or condensed aggregates? Below we argue that the observed properties of the examined GxG peptides allow for an identification of the interactions that promote fibril and condensed phase self-assembly in water and ethanol-water solutions. More specifically, the observed properties of the aromatic guest residues H, Y, W, F, and Y allow for an evaluation of $\pi\pi$ interactions, while properties of A, D, K, and Y guest residues evaluate the role of hydrogen bonding and van der Waals interactions. Finally, GVG and GPG act as controls where the respective side chain do not promote peptide aggregation. We begin with the discussion on the importance of $\pi\pi$ interactions.

Many reported studies on ultrashort peptides suggest that fibrilization and subsequent gelation requires aromatic residues.[30,61,72] While GHG falls into this category, its propensity for aggregation is predicted to be significantly low when flanked by unsupportive glycine residues.[32] Furthermore, GAG clearly forms crystalline fibrils and gels without the presence of an aromatic side chain. However, our experimental results confirm the importance of aromatic acid residues for self-assembly and gelation in water.

38

In other words, for GxG peptides, only peptides with aromatic guest residues, i.e., GHG, GYG, GWG and GFG, were observed to form long crystalline fibrils that percolate into a network, while the non-aromatic peptides GGG, GVG, GPG, and GKG showed no signs of self-assembly. One exception was GDG, which self-assembled into dense fluffy crystalline aggregates, but was incapable of forming large, visible crystalline fibrils. It is likely that the self-assembly of these peptides involve side chain hydrogen bonding. In its protonated state the aspartate side chain can form hydrogen bonds with practically all functional groups of the peptide. Furthermore, the aromatic peptide GYG was incapable of forming long crystalline fibrils, but rather formed only dense aggregates. In both cases, liquid-liquid phase separation precedes self-assembly. The peculiar behavior of GYG might be attributed to a competition between ππ-stacking and intermolecular hydrogen bonding between the hydroxyl group of tyrosine and the carboxylate group of an adjacent peptide in the unit cell (see Figure 9).

Taken together, our observations suggest that for ultrashort peptides ππ-stacking between aromatic side chains is a decisive promotor of long fibril self-assembly in water,

which is a pre-requisite for sub-molar gelation. However, while $\pi - \pi$ interactions seem essential for fibril self-assembly of GxG peptides in water, self-assembly along other interaction pathways should not be excluded. For example, hydrogen bonding between carbonyl and amide groups, between peptide functional and terminal groups as well as hydrogen bonding and salt bridges between terminal carboxylate and ammonia groups can potentially contribute to fibril-forming intermolecular interactions between the investigated tripeptides.[56] Note that GVG and GPG are not capable of interactions via the guest residue. Therefore, the fact that no self-assembly was observed suggests that hydrogen bonding of only the terminal or the end-peptide groups, or both without the support of interactions between side chains are not sufficient to induce self-assembly into either the fibril or condensate phase. For GAG, the alanine side chain is known to promote stacking between different sheets[73–75] which might be more difficult for the more space filling valine residue.

The importance of hydrogen bonding for peptide self-assembly is demonstrated by the ability of GDG to self-assemble even in water. As discussed above, the self-assembly

40

of GDG in water occurs in a narrow pH interval which corresponds to the deprotonated

C-terminal carboxylate and the protonated aspartate side chain. The pK of the latter is

higher (4.55 for the AD dipeptide) than the pK-value of the former which generally lies

between 2.5 and 4.[57] This narrow range makes sense, since a deprotonated side chain

would add repulsive interactions that generally inhibit self-assembly.[20,43] Figure S3

clearly indicates that the self-assembled GDG crystalline structure in water and that of

pure peptide are indistinguishable, and therefore GDG self-assembly in water occurs via

hydrogen bonding between the aspartate side chain (donor) and the carboxylate C-

terminal (acceptor). The crystal structure in the unit cell suggests additional hydrogen

bonding between terminal groups as well as between terminal and peptide group. Upon

solvation in water all these interactions have to compete with peptide-water hydrogen

bonding as well as turn-supporting intrapeptide hydrogen bonding[76,77] which might

prevent the formation of crystalline fibrils that are sufficiently long for the formation of the

typical GxG gel phase.

41

The situation is quite different in the presence of water-ethanol, where both GDG and GAG form long crystalline fibrils that are capable of network formation and gelation (Figure 2). It is logical to attribute the different behavior in water and water-ethanol to the rather different hydrogen bonding capabilities of water and ethanol. For example, an addition of ethanol to N'-methylacetamide in water leads to a significant blueshift of the amide I band in the peptide's IR spectrum which is clearly indicative of weaker solute-solvent hydrogen bonding.[78] In such a case interpeptide hydrogen bonding becomes competitive. The self-assembly of GAG into crystalline fibrils was previously argued to occur at the interface between ethanol and water, which allows for the arrangement of GAG into such a way that a different crystalline structure is permitted compared to the crystallization of the pure peptide, see comparison of GAG gel and pure peptide XRD patterns in Figure S3. In other words, the pure peptide powder seems to form hydrogen bonds between terminal ends, which leads to large aggregates, but no long fibril formation. However, the presence of ethanol, allows for a different hydrogen bonding structure to form, which is capable of long fibril formation. This clearly indicates that

42

hydrogen bonding alone can promote fibril formation. While it is not yet clear as to the

unit cell structure of GAG and GDG in the water-ethanol case, a comparison of the GDG

self-assembled structure in water and water-ethanol should lead to a better understanding

of the hydrogen bonding pairs needed for fibril formation. This is the subject of ongoing

research.

One might suspect that increasing hydrophobicity of GxG side chains might

increase their capability to self-assemble into crystalline fibrils. However, this does not

seem to be the case. For example, valine did not self-assemble under any conditions

investigated and ranks considerably higher in hydrophobicity on the Kyte-Doolittle

hydropathy scale when compared to F,[79] which readily self-assembles in water.

Therefore, we can conclude that hydrophobic interactions are not enough to drive self-

assembly. For the aromatic residues, we note a Kyte-Doolittle ranking of F, W, Y, and H

from most hydrophobic to least. Since all are capable of $\pi\pi$ interactions, we might expect

that F self-assembles at significantly lower concentration than histidine or produces more

fibrils at the same peptide concentration than histidine. We acknowledge that the Kyte-

Doolittle is one of many scales available that rank peptide hydrophobicity, and therefore any correlation is specific to the scale chosen. However, if we consider the Kyte-Doolittle scale, the fact that GFG forms significantly denser networks compared to GYG and GHG, denoted by having the highest storage modulus, may suggest that higher hydrophobic guest residues self-assemble into more fibrils for the same peptide concentration. While the data may suggest a correlation between hydrophobicity and network morphology, it is important to consider that any correlation of hydrophobicity of the guest residue and network properties requires significantly more detailed information (i.e. phase diagrams, analysis of crystal structures) than presented in this study.

The incapability of GVG, GKG and GPG to self-assemble in both, water and water-ethanol deserves some additional thoughts. A probable reason is obvious for GPG, for where the capability of the N-terminal peptide group to form intermolecular hydrogen bonding is substantially reduced. In addition, the proline side chain imposes a high propensity for polyproline II[80] which might not be an ideal conformation for the formation of crystalline fibrils. As indicated above the self-assembly of GVG might be prevented by

44

steric interactions. The rather bulky side chain of valine might not easily fit into any of the

unit cells in Figure 9 unless the peptide adopts a sterically forbidden conformation. The

latter might lack any stabilizing interactions because the side chains cannot accept or

donate hydrogen bonds. Lysine as side chains might be equally prohibitive. Moreover, its

positive charge is also likely to contribute to repulsive forces.[21] Contrary to GVG and

GKG, the guest residue of GDG is not very sterically demanding and possess hydrogen

donor and acceptor capacity in its protonated state.

Conclusions

The investigated GxG peptides can be considered miniature models of intrinsically

disordered proteins involved in intracellular phase separation processes. Thus, they serve

as models for understanding the interactions that are necessary to induce self-assembly,

and more specifically fibril self-assembly. The present study reveals that aromaticity of

the host residue is a requirement for GxG peptides to self-assemble into crystalline fibrils

in water. This can be equally attributed to the strength of ππ- interactions and their

capability to impose a high degree of order.[61] This is in strong support of theoretical

45

results, which list aromaticity as the strongest proponent for fibril self-assembly. Moreover, our data suggest that aromatic residues can promote the formation of crystalline fibrils even in absence of supporting nearest neighbors, which seems to be at variance with theory-based propensities depicted in ref.[32], which suggest that e.g. GFG is less likely to self-assemble in comparison with FFG, FFC or FFA.   Hydrogen bonding guest residues can only form self-assembled dense aggregates in water. Interestingly, non-aromatic hydrogen bonding guest peptides can self-assemble in water into crystalline fibrils in the presence of a cosolvent, such as ethanol. This could be due to the lower hydrogen bond strength between peptides and ethanol (compared to water), which makes interpeptide hydrogen bonding more competitive. Note that the XRD pattern of non-aromatic hydrogen bonding guest residue fibrils formed in co-solvent are different from that of the pure peptide powder formed in pure water, suggesting the importance of unique conformational unit cells promoted by the cosolvent. Finally, the data suggests that hydrophobic interactions are not a driving force for fibril self-assembly, but may play a role in the network properties.   Overall, these results on short tri-peptides elucidate a

46

series of empirical interaction rules for short peptide fibril self-assembly, and may also prove useful in understanding the self-assembly of longer peptides. Furthermore, we expect these results will be useful for comparison to future theoretical simulations involving both pH induced and co-solvent induced peptide self-assembly.

Acknowledgements

References

1. Lin BF, Megley KA, Viswanathan N, et al. PH-responsive branched peptide amphiphile hydrogel designed for applications in regenerative medicine with potential as injectable tissue scaffolds. *J Mater Chem*. 2012;22(37):19447-19454. doi:10.1039/c2jm31745a

2. Measey TJ, Schweitzer-Stenner R. Self-Assembling Alanine-Rich Peptides of Biomedical and Biotechnological Relevance. In: Schweitzer-Stenner R, ed. *Protein and Peptide Folding, Misfolding, and Non-Folding*. Hoboken: Wiley & Sons; 2012:307-350. doi:10.1002/9781118183373.ch11

3. Colombo G, Soto P, Gazit E. Peptide self-assembly at the nanoscale: a challenging target for computational and experimental biotechnology. *Trends Biotechnol*. 2007;25(5):211-218. doi:10.1016/j.tibtech.2007.03.004

4. Draper ER, Adams DJ. Low-Molecular-Weight Gels: The State of the Art. *Chem*. 2017;3:390-410.

5.   Beebe DJ, Moore JS, Bauer JM, et al. Functional hydrogel structures for autonomous flow control inside microfluidic channels. *Nature*. 2000;404(6778):588-590. doi:10.1038/35007047

6.   Aggeli A, Bell M, Boden N, et al. Responsive gels formed by the spontaneous self-assembly of peptides into polymeric β-sheet tapes. *Nature*. 1997;386(6622):259-262. doi:10.1038/386259a0

7.   Reches M, Gazit E. Casting metal nanowires within discrete self-assembled peptide nanotubes. *Science (80-)*. 2003;300(5619):625-627. doi:10.1126/science.1082387

8.   Schweitzer-Stenner R, Alvarez NJ. Short Peptides as Tunable, Switchable, and Strong Gelators. *J Phys Chem B*. 2021;125(25):6760-6775. doi:10.1021/acs.jpcb.1c01447

9.   Holmes TC, De Lacalle S, Su X, Liu G, Rich A, Zhang S. Extensive neurite outgrowth and active synapse formation on self-assembling peptide scaffolds. *Proc Natl Acad Sci U S A*. 2000;97(12):6728-6733. doi:10.1073/pnas.97.12.6728

49

10.   Holmes TC. Novel peptide-based biomaterial scaffolds for tissue engineering.

       Trends Biotechnol. 2002;20(1):16-21. doi:10.1016/S0167-7799(01)01840-6

11.   Adler-Abramovich L, Gazit E. Correction: The physical properties of supramolecular

       peptide assemblies: From building block association to technological applications.

       Chem Soc Rev. 2014;43(20):7236-7236. doi:10.1039/c4cs90080d

12.   Seow WY, Hauser CAE. Short to ultrashort peptide hydrogels for biomedical uses.

       Mater Today. 2014;17(8):381-388. doi:10.1016/j.mattod.2014.04.028

13.   Xu G, Wang W, Groves JT, Hecht MH. Self-assembled monolayers from a

       designed combinatorial library of de novo β-sheet proteins. *Proc Natl Acad Sci U S

       A*. 2001;98(7):3652-3657. doi:10.1073/pnas.071400098

14.   Rajagopal K, Schneider JP. Self-assembling peptides and proteins for

       nanotechnological applications. *Curr Opin Struct Biol*. 2004;14(4):480-486.

       doi:10.1016/j.sbi.2004.06.006

15.   Ye Z, Zhang H, Luo H, et al. Temperature and pH effects on biophysical and

morphological properties of self-assembling peptide RADA 16-1. *J Pept Sci*. 2008;14(2):152-162. doi:10.1002/psc.988

16. Nagai Y, Unsworth LD, Koutsopoulos S, Zhang S. Slow release of molecules in self-assembling peptide nanofiber scaffold. *J Control Release*. 2006;115(1):18-25. doi:10.1016/j.jconrel.2006.06.031

17. Yokoi H, Kinoshita T, Zhang S. Dynamic reassembly of peptide RADA16 nanofiber scaffold. *Proc Natl Acad Sci U S A*. 2005;102(24):8414-8419. doi:10.1073/pnas.0407843102

18. Zhang S, Lockshin C, Cook R, Rich A. Unusually stable β-sheet formation in an ionic self-complementary oligopeptide. *Biopolymers*. 1994;34(5):663-672. doi:10.1002/bip.360340508

19. Wang J, Tang F, Li F, et al. The Amphiphilic Self-Assembling Peptide EAK16-I as a Potential Hydrophobic Drug Carrier. *J Nanomater*. 2008;2008:1-8. doi:10.1155/2008/516286

20.   Ozbas B, Kretsinger J, Rajagopal K, Schneider JP, Pochan D. Salt-triggered

      peptide folding and consequent self-assembly into hydrogels with tunable modulus.

      Macromolecules. 2004;37:7331-7337.

21.   Schneider JP, Pochan DJ, Ozbas B, Rajagopal K, Pakstis L, Kretsinger J.

      Responsive hydrogels from the intramolecular folding and self-assembly of a

      designed   peptide.   *J   Am   Chem   Soc*.   2002;124(50):15030-15037.

      doi:10.1021/ja027993g

22.   Measey T, Schweitzer-Stenner R. The conformations adopted by the octamer

      peptide (AAKA)2 in aqueous solution probed by FTIR and polarized Raman

      spectroscopy. *J Raman Spectrosc*. 2006;37(1-3):248-254. doi:10.1002/jrs.1455

23.   Measey TJ, Schweitzer-Stenner R, Sa V, Kornev K. Anomalous conformational

      instability and hydrogel formation of a cationic class of self-assembling

      oligopeptides. *Macromolecules*. 2010;43(18):7800-7806. doi:10.1021/ma101450b

24.   DiGuiseppi D, Kraus J, Toal SE, Alvarez N, Schweitzer-Stenner R. Investigating

52

the Formation of a Repulsive Hydrogel of a Cationic 16mer Peptide at Low Ionic Strength in Water by Vibrational Spectroscopy and Rheology. *J Phys Chem B*. 2016;120(38):10079-10090. doi:10.1021/acs.jpcb.6b07673

25.   Gazit E. Self Assembly of short Aromatic Peptide into Amyloid Fibrils and Related Nanostructures. *Prion*. 2007;1:32-35.

26.   Görbitz CH. The structure of nanotubes formed by diphenylalanine, the core recognition motif of Alzheimer's β-amyloid polypeptide. *Chem Commun*. 2006;(22):2332-2334. doi:10.1039/b603080g

27.   Makin OS, Atkins E, Sikorski P, Johansson J, Serpell LC. Molecular basis for amyloid fibril formation and stability. *Proc Natl Acad Sci U S A*. 2005;102(2):315-320. doi:10.1073/pnas.0406847102

28.   Gazit E. Self assembly of short aromatic peptides into amyloid fibrils and related nanostructures. *Prion*. 2007;1(1):32-35. doi:10.4161/pri.1.1.4095

29.   Reches M, Porat Y, Gazit E. Amyloid fibril formation by pentapeptide and

tetrapeptide fragments of human calcitonin. *J Biol Chem*. 2002;277(38):35475-35480. doi:10.1074/jbc.M206039200

30.   Tao K, Levin A, Adler-Abramovich L, Gazit E. Fmoc-modified amino acids and short peptides: Simple bio-inspired building blocks for the fabrication of functional materials. *Chem Soc Rev*. 2016;45(14):3935-3953. doi:10.1039/c5cs00889a

31.   Fleming S, Ulijn R V. Design of nanostructures based on aromatic peptide amphiphiles. *Chem Soc Rev*. 2014;43(23):8150-8177. doi:10.1039/c4cs00247d

32.   Frederix PWJM, Scott GG, Abul-Haija YM, et al. Exploring the sequence space for (tri-)peptide self-assembly to design and discover new hydrogels. *Nat Chem*. 2015;7(1):30-37. doi:10.1038/nchem.2122

33.   Farrell S, DiGuiseppi D, Alvarez N, Schweitzer-Stenner R. The interplay of aggregation, fibrillization and gelation of an unexpected low molecular weight gelator: Glycylalanylglycine in ethanol/water. *Soft Matter*. 2016;12(28):6096-6110. doi:10.1039/c6sm00879h

54

34. Milorey B, Farrell S, Toal SE, Schweitzer-Stenner R. Demixing of water and ethanol
     causes conformational redistribution and gelation of the cationic GAG tripeptide.
     Chem Commun. 2015;51(92):16498-16501. doi:10.1039/c5cc06097d

35. Thursch LJ, DiGuiseppi D, Lewis TR, Schweitzer-Stenner R, Alvarez NJ. Exploring
     the gel phase of cationic glycylalanylglycine in ethanol/water. I. Rheology and
     microscopy studies. *J Colloid Interface Sci*. 2020;564(in press):499-509.
     doi:10.1016/j.jcis.2019.10.029

36. Hesser M, Thursch L, Lewis T, DiGuiseppi D, Alvarez NJ, Schweitzer-Stenner R.
     The tripeptide GHG as an unexpected hydrogelator triggered by imidazole
     deprotonation. *Soft Matter*. 2020;16(17):4110-4114. doi:10.1039/d0sm00224k

37. Kurouski D, Dukor RK, Lu X, Nafie LA, Lednev IK. Normal and reversed
     supramolecular chirality of insulin fibrils probed by vibrational circular dichroism at
     the protofilament level of fibril structure. *Biophys J*. 2012;103(3):522-531.
     doi:10.1016/j.bpj.2012.04.042

55

38.   Measey TJ, Schweitzer-Stenner R. Vibrational circular dichroism as a probe of fibrillogenesis: The origin of the anomalous intensity enhancement of amyloid-like fibrils. *J Am Chem Soc*. 2011;133(4):1066-1076. doi:10.1021/ja1089827

39.   Draper ER, McDonald TO, Adams DJ. A low molecular weight hydrogel with unusual gel aging. *Chem Commun*. 2015;51(30):6595-6597. doi:10.1039/c5cc01334h

40.   Mallia VA, Butler PD, Sarkar B, Holman KT, Weiss RG. Reversible phase transitions within self-assembled fibrillar networks of (R)-18-(n - alkylamino)octadecan-7-ols in their carbon tetrachloride gels. *J Am Chem Soc*. 2011;133(38):15045-15054. doi:10.1021/ja204371b

41.   Jentzen W, Unger E, Karvounis G, Shelnutt JA, Dreybrodt W, Schweitzer-Stenner R. Conformational properties of nickel(II) octaethylporphyrin in solution. 1. Resonance excitation profiles and temperature dependence of structure-sensitive Raman lines. *J Phys Chem*. 1996;100(33):14184-14191. doi:10.1021/jp9533032

42.　Thursch LJ, DiGuiseppi D, Lewis TR, Schweitzer-Stenner R, Alvarez NJ. Exploring

the gel phase of cationic glycylalanylglycine in ethanol/water. I. Rheology and

microscopy studies. *J Colloid Interface Sci*. 2020;564.

doi:10.1016/j.jcis.2019.10.029

43.　Tang C, Smith AM, Collins RF, Ulijn R V., Saiani A. Fmoc-Diphenylalanine Self-

ASsembly Mechanism Induces Apparent pK a Shifts. *Langmuir*. 2009;25(16):9447-

9453. doi:10.1021/la900653q

44.　Singh G, Brovchenko I V., Oleinikova A, Winter R. Peptide aggregation in finite

systems. *Biophys J*. 2008;95(7):3208-3221. doi:10.1529/biophysj.108.136226

45.　Hesser M, Thursch LJ, Lewis TR, Lima TA, Alvarez NJ, Schweitzer-Stenner R.

Concentration Dependence of a Hydrogel Phase Formed by the Deprotonation of

the Imidazole Side Chain of Glycylhistidylglycine. *Langmuir*. 2021;37(23):6935-

6946. doi:10.1021/acs.langmuir.1c00382

46.　DiGuiseppi D, Schweitzer-Stenner R. Probing conformational propensities of

57

histidine in different protonation states of the unblocked glycyl-histidyl-glycine peptide by vibrational and NMR spectroscopy. *J Raman Spectrosc*. 2016;47(9):1063-1072. doi:10.1002/jrs.4885

47. Toal SE, Verbaro DJ, Schweitzer-Stenner R. Role of enthalpy-entropy compensation interactions in determining the conformational propensies of amino acid residues in unfolded peptides. *J Phys Chem B*. 2014;118(5):1309-1318. doi:10.1021/jp500181d

48. Harmon TS, Holehouse AS, Rosen MK, Pappu R V. Intrinsically disordered linkers determine the interplay between phase separation and gelation in multivalent proteins. *Elife*. 2017;6:e30294. doi:10.7554/eLife.30294

49. DiGuiseppi DM, Thursch L, Alvarez NJ, Schweitzer-Stenner R. Exploring the gel phase of cationic glycylalanylglycine in ethanol/water. II. Spectroscopic, kinetic and thermodynamic studies. *J Colloid Interface Sci*. 2020;573(subsequent paper in this issue):123-134. doi:10.1016/j.jcis.2020.03.108

50.   Schweitzer-Stenner R. The combined use of amide I bands in polarized Raman,

       IR, and vibrational dirchroism spectra for the structure analysis of peptide fibrils and

       disordered peptided and proteins. *J Raman Spectrosc.* 2021;52:2479-2499.

51.   Karjalainen EL, Ravi HK, Barth A. Simulation of the amide I absorption of stacked

       β-sheets. *J Phys Chem B.* 2011;115(4):749-757. doi:10.1021/jp109918c

52.   Lee C, Cho M. Local amide I mode frequencies And coupling constants in multiple-

       stranded antiparallel β-sheet polypeptides. *J Phys Chem B.* 2004;108(52):20397-

       20407. doi:10.1021/jp0471204

53.   Schweitzer-Stenner R. Simulated IR, isotropic and anisotropic Raman, and

       vibrational circular dichroism amide i band profiles of stacked β-sheets. *J Phys

       Chem B.* 2012;116(14):4141-4153. doi:10.1021/jp2112445

54.   Pajcini V, Chen XG, Bormett RW, et al. Glycylglycine $\pi \rightarrow \pi^*$ and charge transfer

       transition   moment   orientations: Near-resonance   Raman   single-crystal

       measurements. *J Am Chem Soc.* 1996;118(40):9716-9726. doi:10.1021/ja961725z

55.   Ilawe NV, Schweitzer-Stenner R, DiGuiseppi D, Wong BM. Is a cross-β-sheet

structure of low molecular weight peptides necessary for the formation of fibrils and

peptide hydrogels. *Phys Chem Chem Phys*. 2018;20:18158-18168.

56.   O'Neill N, Lima TA, Ferreira FF, Thursch L, Alvarez N, Schweitzer-Stenner R.

Forbidden Secondary Structures Found in Gel-Forming Fibrils of

Glycylphenylalanylglycine. *J Phys Chem B*. 2022;in press.

doi:10.1021/acs.jpcb.2c05010

57.   Dragomir IC, Measey TJ, Hagarman AM, Schweitzer-Stenner R. Environment-

controlled interchromophore charge transfer transitions in dipeptides probed by UV

Absorption and electronic circular dichroism spectroscopy. *J Phys Chem B*.

2006;110(26):13235-13241. doi:10.1021/jp0616260

58.   Sieler G, Schweitzer-Stenner R, Holtz JSW, Pajcini V, Asher SA. Different

conformers and protonation states of dipeptides probed by polarized Raman, UV-

resonance Raman, and FTIR spectroscopy. *J Phys Chem B*. 1999;103(2):372-384.

doi:10.1021/jp9825462

60

59.   Frederix PWJM, Ulijn R V., Hunt NT, Tuttle T. Virtual screening for dipeptide

        aggregation: Toward predictive tools for peptide self-Assembly. *J Phys Chem Lett*.

        2011;2(19):2380-2384. doi:10.1021/jz2010573

60.   Needham TE. The Solubility of Amino Acids in Various Solvent Systems. 170AD.

        https://digitalcommons.uri.edu/oa_diss/159%0A.

61.   Smith AM, Williams RJ, Tang C, et al. Fmoc-diphenylalanine self assembles to a

        hydrogel via a novel architecture based on π-π interlocked β-sheets. *Adv Mater*.

        2008;20(1):37-41. doi:10.1002/adma.200701221

62.   Amdursky N, Gazit E, Rosenman G. Quantum Confinement in Self-Assembled

        Bioinspired Peptide Hydrogels. *Adv Mat*. 2010;22:2311-2315.

63.   Draper ER, Adams DJ. How should multicomponent supramolecular gels be

        characterised? *Chem Soc Rev*. 2018;47(10):3395-3405. doi:10.1039/c7cs00804j

64.   De Leon Rodriguez LM, Hemar Y, Cornish J, Brimble MA. Structure-mechanical

        property correlations of hydrogel forming β-sheet peptides. *Chem Soc Rev*.

2016;45(17):4797-4824. doi:10.1039/c5cs00941c

65.   Yokoi H, Kinoshita T. Strategy for designing self-assembling peptides to prepare

transparent nanofiber hydrogel at neutral pH. *J Nanomater*. 2012;2012:537262.

doi:10.1155/2012/537262

66.   Panda JJ, Mishra A, Basu A, Chauhan VS. Stimuli responsive self-assembled

hydrogel of a low Molecular weight free dipeptide with potential for tunable drug

delivery. *Biomacromolecules*. 2008;9(8):2244-2250. doi:10.1021/bm800404z

67.   Pickup RM, Cywinski R, Pappas C, Farago B, Fouquet P. Generalized Spin-Glass

relaxation. *Phys Rev Lett*. 2009;102:097202.

68.   Movellan KT, Wegstroth M, Overkamp K, Leonov A, Becker S, Andreas LB.

Imidazole-Imidazole Hydrogen Bonding in the pH Sensing Histidine Side Chains of

Influenca A M2. *J Am Chem Soc USA*. 2020;142:2704-2708.

69.   Dégeilh R, Pickworth J. Unit-cell dimensions and space groups of some simple

peptides. *Acta Crystallogr*. 1956;9(10):828-828. doi:10.1107/s0365110x5600231x

70. Marsh RE, Glusker JP. The crystal structure of glycylphenylalanylglycine. *Acta Crystallogr*. 1961;14(11):1110-1116. doi:10.1107/s0365110x61003296

71. Shin Y, Brangwynne CP. Liquid phase condensation in cell physiology and disease. *Science (80-)*. 2017;357(6357):eaaf4382. doi:10.1126/science.aaf4382

72. Mahler A, Reches M, Rechter M, Cohen S, Gazit E. Rigid, self-assembled hydrogel composed of a modified aromatic dipeptide. *Adv Mater*. 2006;18(11):1365-1370. doi:10.1002/adma.200501765

73. Measey TJ, Smith KB, Decatur SM, Zhao L, Yang G, Schweitzer-Stenner R. Self-aggregation of a polyalanine octamer promoted by its C-terminal tyrosine and probed by a strongly enhanced vibrational circular dichroism signal. *J Am Chem Soc*. 2009;131(51):18218-18219. doi:10.1021/ja908324m

74. Nguyen HD, Hall CK. Kinetics of Fibril Formation by Polyalanine Peptides. *J Biol Chem*. 2005;280:9074-9082.

75. Measey TJ, Schweitzer-Stenner R. Vibrational circular dichroism as a probe of

fibrillogenesis: The origin of the anomalous intensity enhancement of amyloid-like fibrils. *J Am Chem Soc*. 2011;133(4):1066-1076. doi:10.1021/ja1089827

76. Rybka K, Toal SE, Verbaro DJ, Mathieu D, Schwalbe H, Schweitzer-Stenner R. Disorder and order in unfolded and disordered peptides and proteins: A view derived from tripeptide conformational analysis. II. Tripeptides with short side chains populating asx and β-type like turn conformations. *Proteins Struct Funct Bioinforma*. 2013;81(6):968-983. doi:10.1002/prot.24226

77. Milorey B, Schwalbe H, O'Neill N, Schweitzer-Stenner R. Repeating Aspartic Acid Residues Prefer Turn-like Conformations in the Unfolded State: Implications for Early Protein Folding. *J Phys Chem B*. 2021;125(41):11392-11407. doi:10.1021/acs.jpcb.1c06472

78. Diguiseppi D, Milorey B, Lewis G, et al. Probing the Conformation-Dependent Preferential Binding of Ethanol to Cationic Glycylalanylglycine in Water/Ethanol by Vibrational and NMR Spectroscopy. *J Phys Chem B*. 2017;121(23):5744-5758. doi:10.1021/acs.jpcb.7b02899

79.   Kyte J, Doolittle RF. A simple method for displaying the hydropathic character of a

protein. *J Mol Biol*. 1982;157(1):105-132. doi:10.1016/0022-2836(82)90515-0

80.   Cowan PM, Mc Gavin S. Structure of Poly-L-Proline. *Nature*. 1955;176:501-503.

Tables

Table 1. Concentration and pH used for aggregation screening of the GXG peptides in water.

Peptide	Concentration (mM)	pH	Aggregates
GFG	98.7	3.96	Yes
GYG	101.5	5.79	Yes
GDG	96.0	3.88	Yes
GWG	71.3 ± 0.4	0.9 ± 0.1	Yes
GPG	110.9 ± 4.7	9.1 ± 3.2	No
GKG	114.2 ± 5.4	8.9 ± 2.7	No
GVG	80	7.0 ± 1.6	No

Table 2. Fits to the IR aggregation kinetic data in Fig.3.Time constant τ was calculated using β^{-1}.

Peptide	Function	Parameters
GFG pH 3.4	$I = I_{max} \cdot \left(1 - e^{-\frac{t}{\tau}}\right)$	I_{max} = 0.121 ± 0.003 τ=21.7 ± 1.2 min
GFG pH 3.8	$I = I_{max} \cdot \left(1 - e^{-\frac{t}{\tau}}\right)$	I_{max} = 0.499±0.005 τ = 0.55±0.07 min

GWG pH 0.7	$I = I_{max,1} \cdot \left(1 - e^{-\frac{t}{\tau_1}}\right) + I_{max,2} \cdot \left(1 - e^{-\frac{t}{\tau_2}}\right)$	$I_{max,1}$ = 0.29 τ_1 = 0.1 min $I_{max,2}$ = 0.29 τ_2 = 0.24±0.03 min[1]
GYG pH 4.1	$I = I_{max} \cdot \left(1 - e^{-\frac{t}{\tau}}\right)$	I_{max} = 0.228 ± 0.007 τ=2.5±0.03 min

[1]Estimated from data scattering. The least square fit did not provide statistical errors. The statistical error for τ_1 is likely to be with the value itself.

Table 3. Fits to the rheology initial formation and reformation data in Fig. 4 and 5.

Sample	G'max (kPa)	+/-	τ (min)	+/-	a	+/-
GFG 100mM	34.4	0.1	10.2	0.1	-2.37	0.05
GFG 100mM (2)	718.8	8.1	7.3	0.1	-3.64	0.05
GFG 100mM (2) reformed	335.8	2.9	23.2	0.1	-4.38	0.04
GFG 200mM	2424.2	6.1	2.0	0.0	-2.22	0.08
GFG 100mM 55mol%	0.55	0.01	20.3	0.8	-1.57	0.09
GWG 75mM	8.84	0.03	46.3	0.1	-3.97	0.04
GWG 100mM	293.8	0.6	15.2	0.1	-3.40	0.04
GYG 100mM	0.41	0.01	37.3	0.9	-1.39	0.03
GYG 200mM	14.68	0.03	8.4	0.1	-2.18	0.04
GYG 200mM (2)	1.46	0.02	12.9	0.2	-3.03	0.08
GYG 200mM (2) reformed	1.24	0.07	25.1	0.6	-4.47	0.17

Table 4. Parameters of the crystalline cells calculated from XRD data.

Sample	System type	Crystalline cell parameters			
		a (Å)	b (Å)	c (Å)	V (Å^3)
GDG powder	Orthorhombic $P2_12_12_1$	17.1256	12.9078	4.75585	1051.30
GFG powder	Orthorhombic $P2_12_12_1$	29.8239	9.9714	4.83616	1438.21
GHG powder	Monoclinic $P2_1$ (β = 104.95°)	11.7071	4.7121	12.4111	661.48
GYG powder	Orthorhombic $P2_12_12_1$	4.8964	9.6784	28.5374	1352.36
GAG powder	Orthorhombic $P2_12_12_1$	12.4827	16.0047	4.74526	948.02

Figures

Figure 1. Molecular structure of the studied GXG peptides with side chain variations.

Figure 2. Microscope images of the hydrogel samples: a) 96 mM GDG pH 4, b) 200 mM GDG pH 4, d) 100 mM GFG pH 4, e) 200 mM GFG pH 3.8, g) 75 mM GWG pH 0.7, h) 200 mM GWG pH 0.7, i) 100 mM GYG pH 4.0, j) 200 mM GYG pH 4.0, k) 75 mM GHG pH 7.1, l) 300 mM GG pH 6.6, and 55 mol% ethanol gels: c) 75 mM GDG, f) 100 mM GFG and m) 220 mM GAG.

Figure 3. IR spectra probing aggregation kinetics for 100 mM gels: a) GFG, pH 3.4, b) GFG, pH 3.8, c) GWG, pH 0.7, and d) GYG pH 4.1.

Figure 4. Normalized integrated fractional intensities of the AI' bands as a function of time obtained by spectral decomposition of the IR data.

Figure 5. Formation kinetics of a) GFG, b) GWG, c) GYG water-based gels monitored by SAOS rheology.

Figure 6. Melting curves of 100 mM GFG, 200 mM GYG, 100 mM GWG and 175 mM

GHG peptides monitored by rheology; formation kinetics of 100 mM GFG and 200 mM

GYG gels at 20°C: initial formation and reformation after an annealing step at 70°C.

Figure 7. Microscope images of 100 mM GFG and 200 mM GYG samples observed

during SAOS. The pictures show initial formation at 20°C and reformation at 20 °C after

an annealing step at 70°C.

Figure 8. XRD data for GAG, GDG, GHG, GFG, GWG, GYG powders and almost dried

100 mM gels (The GAG was ethanol-based and the other one water based-gels). The

data backgrounds and amorphous contribution were removed for better visualization.

Figure 9. Calculated crystalline unit cells of GDG, GHG, GFG, GYG and GAG pure

peptides. The directions a, b and c are represented by red, green and blue, respectively.
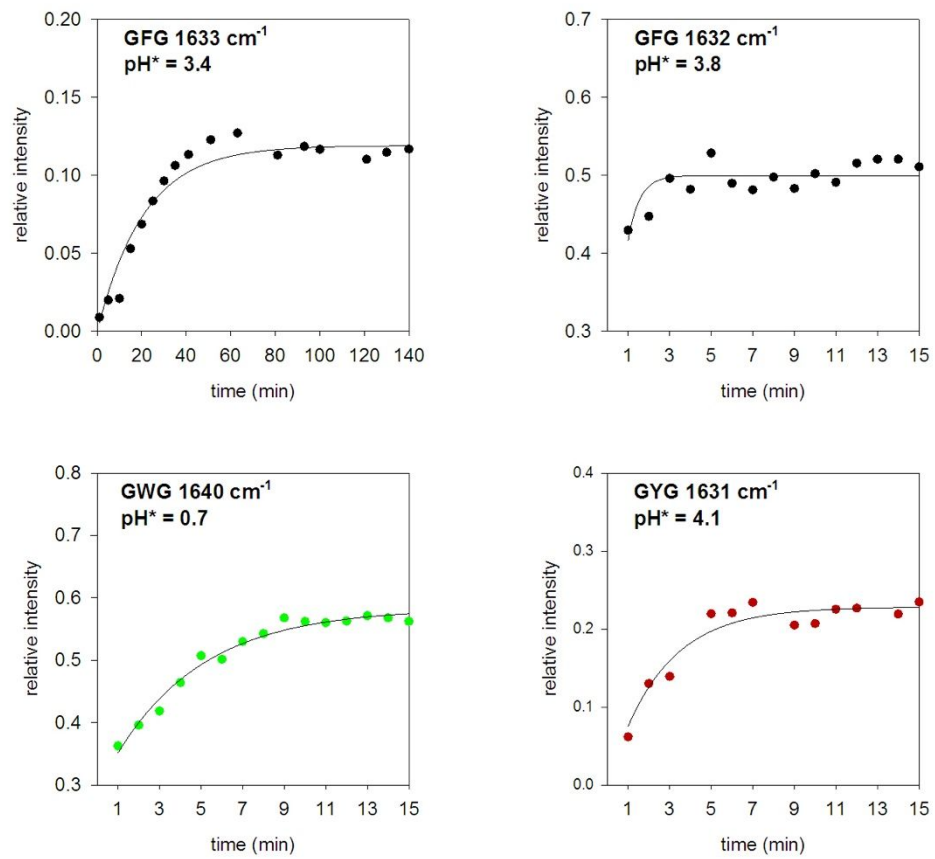
Figure 1
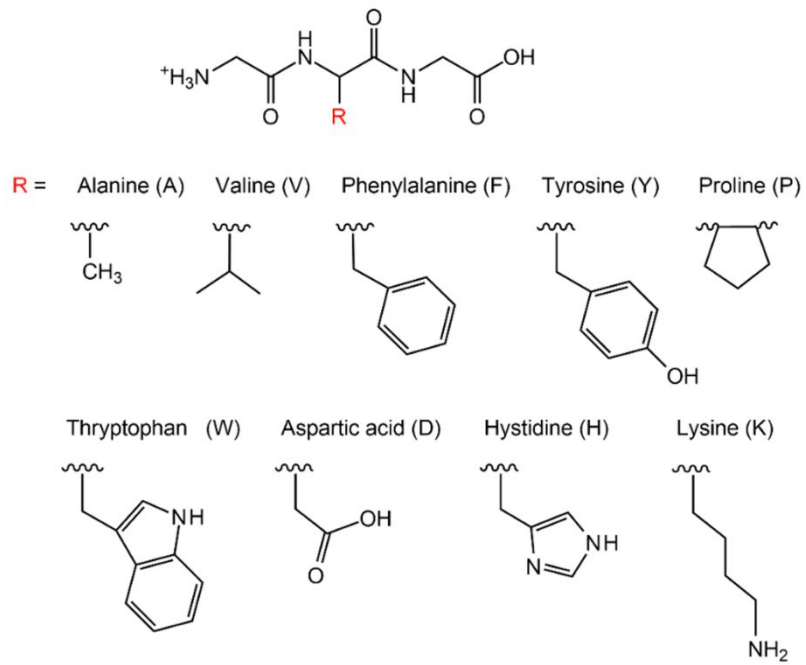
Figure 2
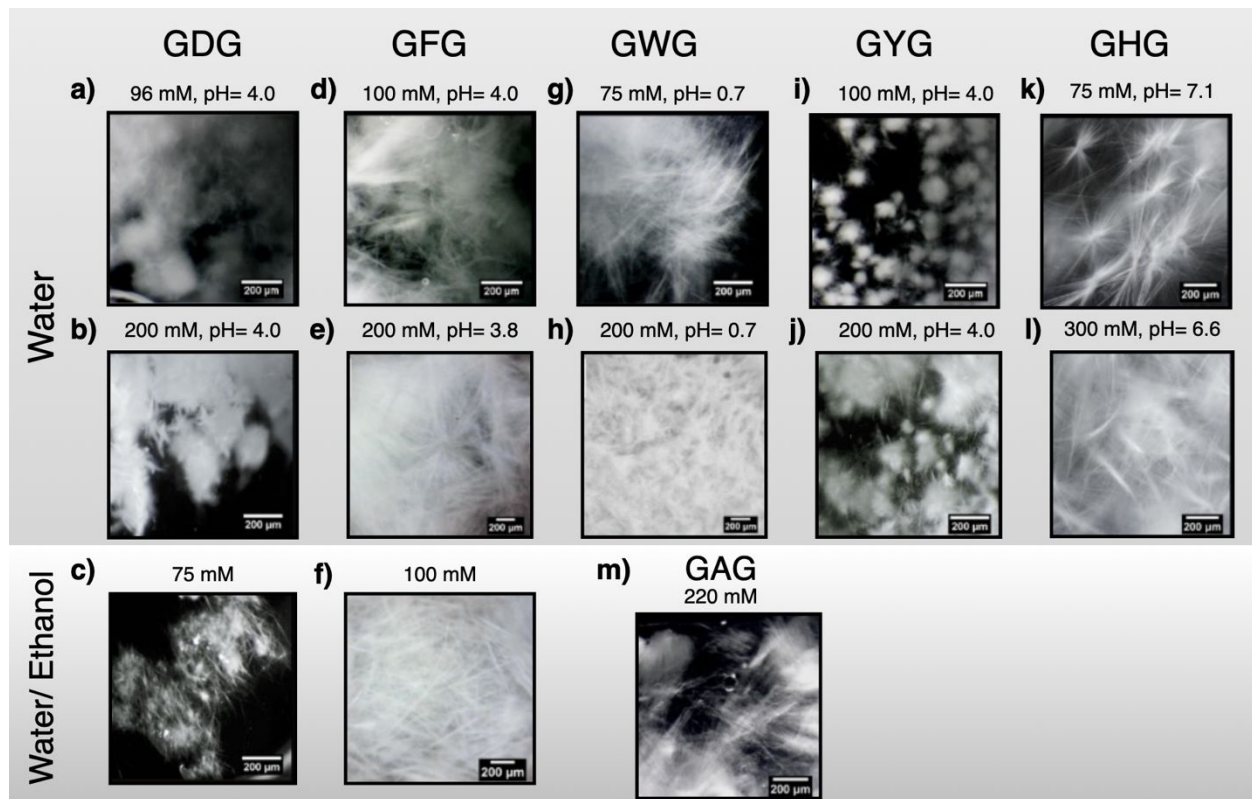
Figure 3

73
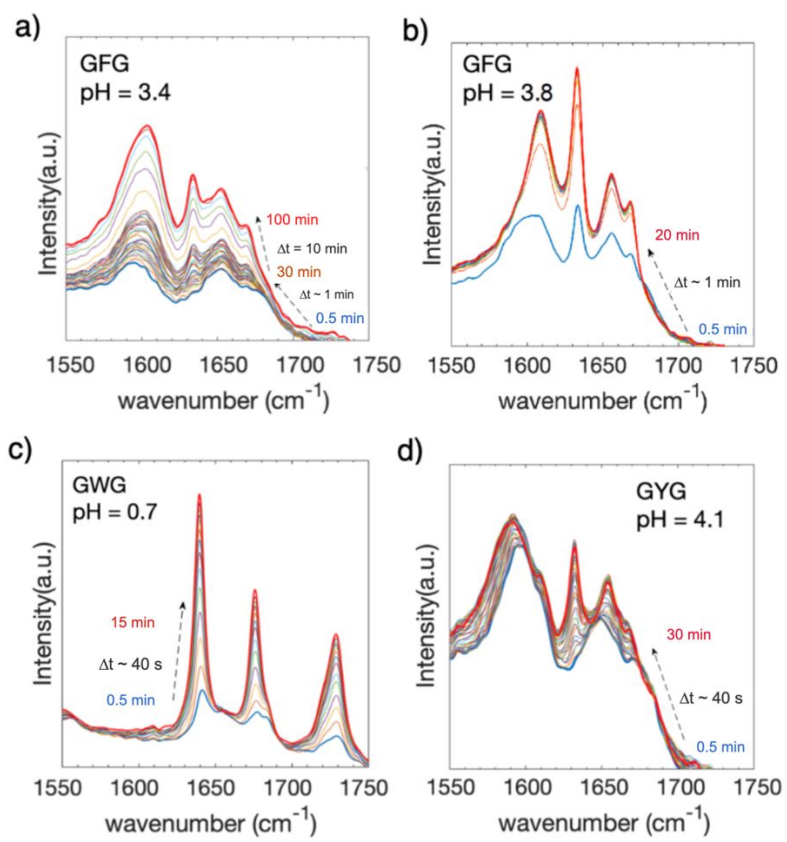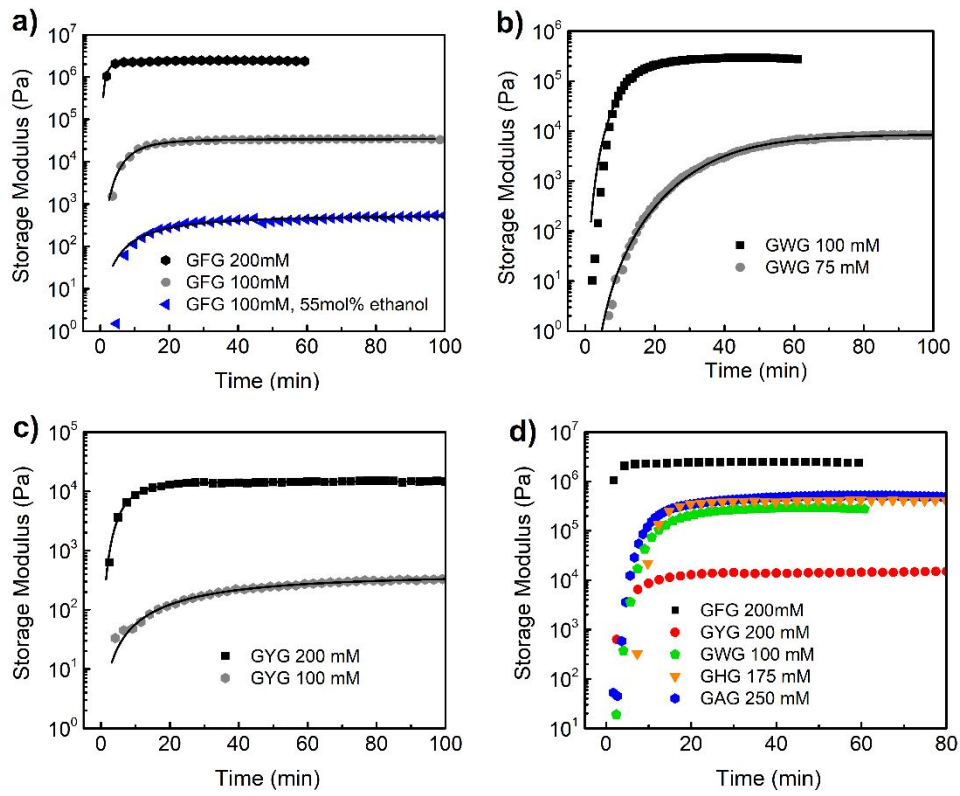
Figure 4

Figure 5

Figure 6
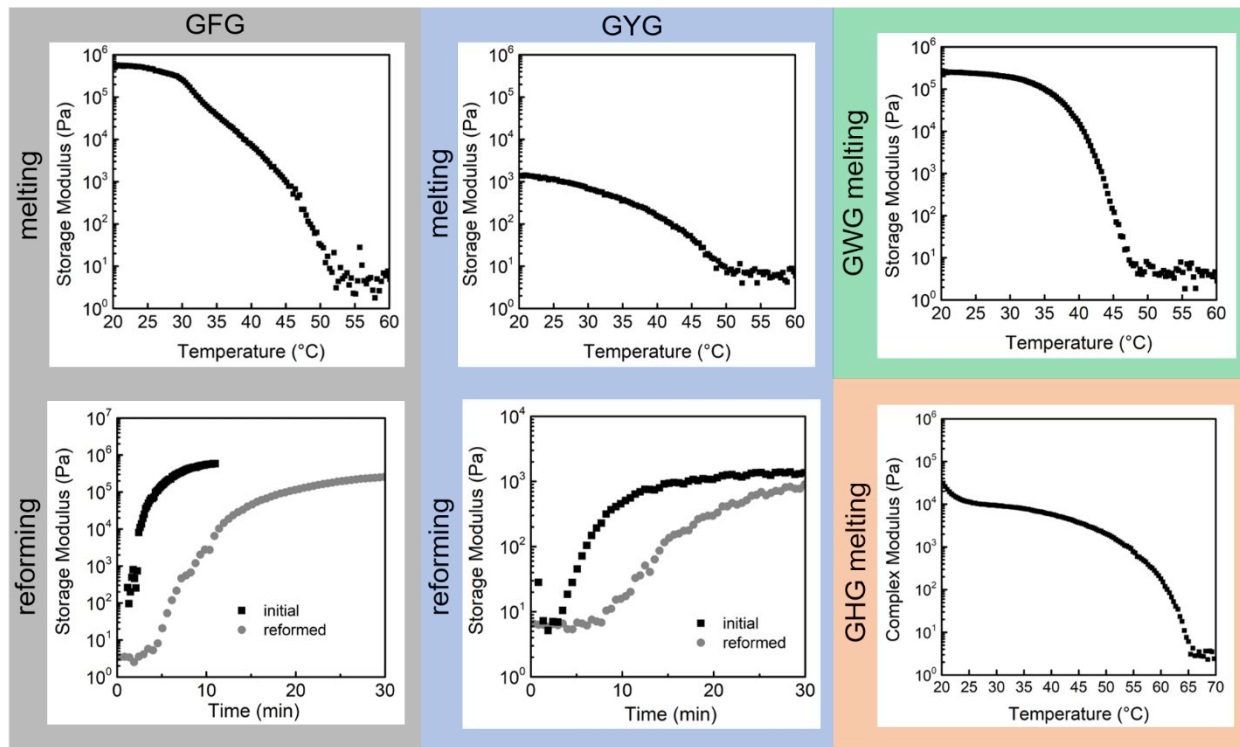
Figure 7

Figure 8

Figure 9